

Binding energies and vibrational spectral features of S_n species on amorphous water-ice mantles: a quantum mechanical study

JESSICA PERRERO,^{1,2} LEIRE BEITIA-ANTERO,^{3,4} ASUNCIÓN FUENTE,⁵ PIERO UGLIENGO,² AND ALBERT RIMOLA¹

¹Departament de Química, Universitat Autònoma de Barcelona, Bellaterra, 08193, Catalonia, Spain

²Dipartimento di Chimica and Nanostructured Interfaces and Surfaces (NIS) Centre, Università degli Studi di Torino, via P. Giuria 7, 10125, Torino, Italy

³AEGORA Research Group - Joint Center for Ultraviolet Astronomy, Universidad Complutense de Madrid, Plaza de Ciencias 3, 28040 Madrid, Spain

⁴Departamento de Estadística e Investigación Operativa, Fac. de CC. Matemáticas, Plaza de Ciencias 3, 28040 Madrid, Spain

⁵Centro de Astrobiología (CSIC/INTA), Ctra. de Torrejón a Ajalvir km 4, E-28806 Torrejón de Ardoz, Spain

ABSTRACT

In the denser and colder regions of the interstellar medium (ISM), gas-phase sulfur is depleted by two or three orders of magnitude with respect to its cosmic abundance. Thus, which species are the main carriers of sulfur is an open question. Recent studies have proposed S_n species as potential sulfur reservoirs. Among the various sulfur allotropes, the most stable one is the S₈ ring, detected in asteroid Ryugu and Orgueil meteorite. Shorter species, namely S₃ and S₄, have been found in comet 67P/C-G, but their presence in the ISM remains elusive. In this study, we compute the binding energies (BEs) of S_n (n=1-8) species on an amorphous water ice surface model and analyze their infrared (IR) and Raman spectral features to provide data for their identification in the ISM. Our computations reveal that these species exhibit lower BEs than previously assumed, and their spectral features experience minimal shifts when adsorbed on water ice because of the weak and non-specific S_n/ice interactions. Furthermore, these species display very low IR band intensities and, therefore, very accurate instruments operating in the mid-infrared range are required for detecting the presence of these species in dense interstellar environments.

Keywords: Unified Astronomy Thesaurus concepts: Surface ices (2117) — Interstellar dust (836) — Interstellar molecules (849) — Dense interstellar clouds (371) — Interstellar medium (847) — Solid matter physics (2090) — Interstellar dust processes (838) — Computational methods (1965)

1. INTRODUCTION

Sulfur chemistry has garnered significant interest in astrochemistry, particularly since sulfur depletion in the interstellar medium (ISM) was first acknowledged in the 1970s (Spitzer & Jenkins 1975; Gondhalekar 1985). Although the abundance of sulfur in the gas phase of the diffuse medium is consistent with the cosmic value, $[S]/[H] = 1.5 \times 10^{-5} \text{ cm}^{-3}$ (Jenkins 2009),

more evolved environments such as translucent clouds and dense clouds are characterized by an environment-dependent depletion of one or two orders of magnitude (Fuente et al. 2023). Initially, the sulfur missing from the gas phase was expected to yield H₂S on the icy grain mantles (Caselli et al. 1994), similar to the freezing of oxygen atoms yielding H₂O. However, the abundance of S-bearing species observed in the ice mantle (OCS, and tentatively SO₂) and the upper limits estimated for H₂S, account for less than 5% of the sulfur budget in the solid phase (Boogert et al. 2022; McClure et al. 2023). For this reason, the main reservoirs of sulfur are still unknown, and its chemistry is being extensively investigated.

Corresponding author: Albert Rimola, Piero Ugliengo
 piero.ugliengo@unito.it

albert.rimola@uab.cat

Sulfur is known to present different molecular allotropes, forming chains and rings up to 20 atoms, as it easily tends to react with itself even in a diluted medium. In the last 20 years, the interest in the S_n species (with $2 \leq n \leq 8$) has grown exponentially in the field of astrochemistry, after being first proposed as S-reservoirs (Wakelam et al. 2004). Several experiments have shown the production of these species, together with H_2S_n (with $n \geq 2$), after photoprocessing of H_2S -containing ices (e.g. Ferrante et al. 2008; Jiménez-Escobar & Caro 2011; Jiménez-Escobar et al. 2014; Cazaux et al. 2022). When including proper reaction pathways, astrochemical models also predict their formation (Laas & Caselli 2019). In particular, when considering cosmic-ray-driven radiation chemistry and fast non-diffusive reactions for bulk radicals, pure sulfur allotropes are one of the main products (Shingledecker et al. 2020). So far, the only molecule characterized by a S–S bond was detected in the Horsehead nebula, a moderately UV-irradiated environment, where gas-phase S_2H was found (Fuente et al. 2017). On the other hand, S_3 and S_4 have been detected in comet 67P/C-G (beside sulfides and sulfur oxides) by Calmonte et al. (2016). In the same source, Altwegg et al. (2022) also detected ammonium sulfide, which is the most abundant salt of the comet. S_n species have also been found in other bodies of the Solar system, such as the Ryugu asteroid and the Orgueil meteorite, which contain low and high abundances of S_8 , respectively (Aponte et al. 2023).

The formation mechanism of S_n species is suspected to depend on the environment. Translucent cloud conditions are more likely to favor the formation of long S_n -species (Cazaux et al. 2022), as Ruffle et al. (1999) suggested that the negative grain charge distribution could be responsible for enhancing S^+ accretion on the core of the grains. On the other hand, laboratory experiments predict the formation of short S_n species due to UV photoprocessing of H_2S ice, along with the formation of H_2S_n species (Jiménez-Escobar & Caro 2011; Jiménez-Escobar et al. 2014). The abundance ratio between the species that are formed depends on the shielding effect of the H_2S ice (Cazaux et al. 2022). S_n ($n > 4$) species would be more refractory as n increases, so that they could not desorb from the core of the grains in hot cores/hot corinos, but could be released in shock regions. On the other hand, S_n ($2 \leq n \leq 4$) species could potentially be observed in less harsh environments, and hence the need for providing spectroscopic data for their identification.

With the launch of JWST in December 2021 and the beginning of the EUCLID mission in July 2023, nu-

merous spectra will be collected, not only for gas-phase species, but also for interstellar ices, and the interpretation of the spectra will need both experimental and computational data.

From a theoretical point of view, there are several studies on the S_n free molecules, which elucidate their geometrical features and electronic states (e.g., Raghavachari et al. 1990; McCarthy et al. 2004a,b). Their IR and Raman spectra have been recorded experimentally in the gas phase or with matrix isolation in solid argon technique, depending on which was more feasible for each species, which are collected in reviews (Eckert & Steudel 2003; Trofimov et al. 2009). Gas-phase S_3 and S_4 have also been characterized by means of rotational spectroscopy in the mm regions, providing valuable data for their detection and identification in the ISM (McCarthy et al. 2004a,b). However, to the best of our knowledge, no previous studies have been conducted for S_n interacting with water ice. Thus, in this work, we focused on the adsorption of S_n ($n=1-8$) species on interstellar water ices (here modeled as an extended periodic amorphous surface) with the aim to provide their binding energies (BEs) and vibrational spectroscopic (IR and Raman) properties computed at a quantum mechanical level. BEs are important parameters used in astrochemical models to describe the chemical evolution of planet-forming environments. Since BEs appear in exponential terms, their accuracy is mandatory to provide sensible results. Additionally, the perturbation of the vibrational IR and Raman bands of the S_n species due to the adsorption at ice will be of great value for their experimental detection in the ISM ices (at least for the IR spectra). In Section 2 we describe the methodology applied in the simulations, and in Section 3 we present the results and a discussion of their implications in the field of astrochemistry. Finally, in Section 4 we summarize our conclusions.

2. METHODOLOGY

All the calculations were performed with the periodic *ab initio* code CRYSTAL17 (Dovesi et al. 2018), which allows simulating systems from zero to three periodic dimensions (i.e., molecules, polymers, surfaces and bulks) and describe the atoms with Gaussian-type orbitals instead of plane waves (as commonly employed in periodic codes). Due to such a feature, our surfaces are slab models to which periodic boundary conditions (PBC) along two directions have been applied, presenting a finite thickness in the non-periodic direction.

After finding the most stable conformer and electronic state of each gas-phase S_n species, we computed their adsorption on a periodic amorphous-like water ice sur-

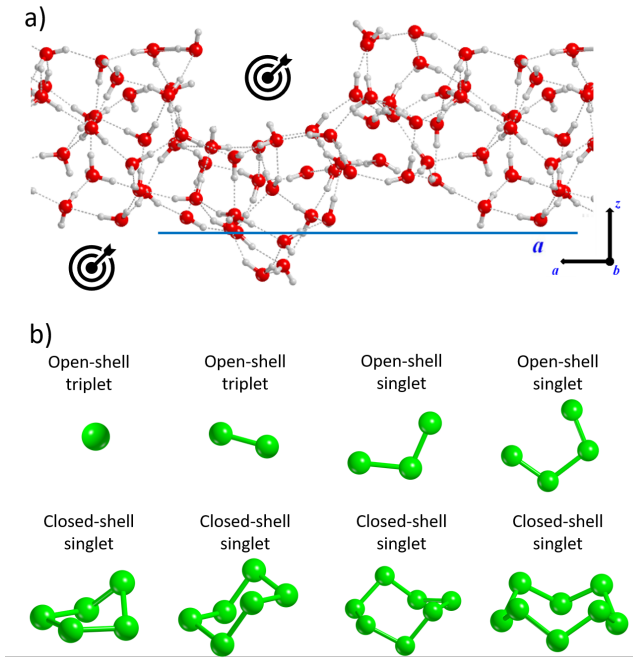


Figure 1. a) Amorphous periodic water ice model adopted in this work. The target icon indicates the binding sites considered for the adsorption of species from S to S₈. Colour code: red, oxygen; grey, hydrogen. b) Species characterized in this work with the corresponding electronic ground state. Species from S to S₄ are linear chains (top row), while species from S₅ to S₈ are cyclic rings (bottom row).

face (see Figure 1). This model was designed by [Ferrero et al. \(2020b\)](#), by joining three amorphous water clusters and applying the PBC, thus cutting the obtained bulk ice model along the (010) plane to yield a periodic surface. The resulting slab was characterized by edges and cavities, with binding sites possessing different adsorption strengths. The distinct morphologies of the upper and lower surfaces are responsible for the presence of a small electric dipole moment across the non-periodic direction. The unit cell has 180 atoms and its cell parameters are $a=20.275$ Å, $b=10.052$ Å, and $\gamma=103.442^\circ$ within the adopted density functional theory (DFT) level (see below).

The geometry optimizations of the gas-phase S_{*n*} species and their adsorption complexes were performed with the hybrid DFT BHLYP functional ([Becke 1993](#); [Lee et al. 1988](#)), supplemented with the D3(BJ) dispersion correction by [Grimme et al. \(2010\)](#) and combined with the Ahlrichs-VTZ* (A-VTZ*) basis set, previously adopted in [Ferrero et al. \(2020b\)](#) and [Perrero et al. \(2022\)](#). The choice of this functional was justified by the need to treat both closed-shell and open-shell species at the highest cost-effective ratio. Thus, we relied on the known good performance of the B3LYP functional

in similar previous publications ([Ferrero et al. 2020b](#); [Perrero et al. 2022](#)) and chose to use a higher percentage of exact exchange (50%) to properly describe open-shell species, resulting in the adoption of the BHLYP-D3(BJ)/A-VTZ* methodology.

The adsorption complexes were computed by relaxing both the internal atomic positions and the unit cell parameters. We selected two binding sites on the amorphous ice model in order to represent the two main binding sites that this model offers: i) the cavity region, and ii) a flat portion of the surface. In the previous works of [Ferrero et al. \(2020b\)](#) and [Perrero et al. \(2022\)](#), more binding sites were probed, with the aim to define BE ranges for a larger set of species which were, however, relatively small in size. In this case, since large non-polar species are involved (interacting mainly through weak non-specific forces), we suppose these two binding sites to be representative of the range of interactions between the molecule and the ice surface. We expect larger BEs for species adsorbed in the cavity region rather than in the flat region because of the larger contact surface between the adsorbate and the ice water molecules (and hence larger interactions), in the former case.

The final binding energies, BE(0), were computed through the equation:

$$BE(0) = BE - \Delta ZPE = -(\Delta E - BSSE) - \Delta ZPE \quad (1)$$

where the interaction energy $\Delta E = E_{complex} - E_{ice} - E_{species}$ was corrected for the basis set superposition error (BSSE, arising from the finiteness of the basis set) and for the zero-point energy ($\Delta ZPE = ZPE_{complex} - ZPE_{ice} - ZPE_{species}$) computed at 0 Kelvin. The ice surface taken as reference is the one optimized after the desorption of the adsorbate, this way neglecting spurious effects in the BE(0)s due to an over-deformation of the ice structure induced by the presence of the adsorbate and caused by the finite thickness of the ice model. Indeed, our experience indicates that an amorphous ice surface, contrary to a rigid crystalline one, can dramatically reconstruct locally to better accommodate the adsorbate ([Perrero et al. 2022](#); [Perrero et al. 2023](#)). The significant deformation observed is the result of fully relaxing the geometry of the systems (both internal atomic positions and unit cell parameters), which is compulsory to ensure that the adsorption complexes are actual minima stationary points, and hence to accurately compute IR and Raman spectra. Consequently, during the optimization process, the ice unit cell may contract or expand, contrary to what would happen on a real ice surface. To address this discrepancy, we opted to derive binding energies from simulations of desorption processes. Basically, we simulate a desorption process rather than

an adsorption one, in which, on the latter the reference surface is the pristine one, while for the former it is the one left after desorption. The different terms that contribute to the BE(0) were analyzed and explained in the Appendix (see Section B), and for their detailed explanation, we refer the reader to the works of [Ferrero et al. \(2020b\)](#) and [Perrero et al. \(2022\)](#).

Frequency calculations on the BHYLP-D3(BJ)/AVTZ*-optimized geometries were run on the adsorption complexes with the twofold aim: i) confirming their nature of minima on the potential energy surface (PES), and ii) computing the IR and Raman spectra. The Hessian matrix was calculated considering only the displacements of the S_n adsorbed species, while the rest of the system is kept at fixed geometry. We previously checked that the exclusion of water molecules did not have a significant influence on the fragment Hessian matrix and, therefore, on the final vibrational spectra. For each coordinate, two displacements along each of the three cartesian coordinates were computed, with a step of 0.001 Å and a tolerance on the SCF energy of 10^{-11} atomic units. Both the IR and Raman intensities were computed through a Coupled-Perturbed Hartree-Fock/Kohn-Sham approach ([Pascale et al. 2004](#); [Zicovich-Wilson et al. 2004](#)), which allows for a completely analytical calculation of Born charges, IR intensities, and dielectric and Raman tensors. Please, note that although we used a fragment to calculate the frequencies involving only the S atoms of the S_n species, the IR and Raman intensities are unaffected by this approach. Indeed, for the IR spectra, the transition dipole moment governing their intensities is calculated through a wave function encompassing the whole system, which accordingly accounts for the polarization effects of the ice. Similarly for the Raman intensities, as the transition polarizability is calculated with the complete wave function. The vibrational modes were classified through the analyzer implemented in CRYSTAL17. The software decomposes the motion of each couple of atoms into three components: the first along the two atoms; the second on the plane containing a third atom; the third out of the above-mentioned plane. Finally, it uses this information to classify the modes as stretching (S), bending (B) or other (O). The IR and Raman spectra were calculated by raw superposition of Lorentzian peaks, with a FWHM of 8 cm⁻¹, applying a Lorentzian broadening to the peaks after computing their relative intensities ([Maschio et al. 2013a,b](#)).

3. RESULTS & DISCUSSION

3.1. *Gas-phase S_n species*

Numerous studies in the literature have delved into the various molecular allotropes of sulfur. These investigations focused not only on the structural features and electronic states of the S_n species but also on their spectroscopic properties. The electronic ground state of atomic sulfur and S_2 is a triplet (like atomic oxygen and O_2), while species with $n \geq 6$ are closed-shell monocyclic rings, which have been characterized by X-ray crystallography and infrared spectroscopy ([Eckert & Steudel 2003](#)). However, the S_3 , S_4 and S_5 systems have sparked debates regarding their configuration as either chains or rings, prompting extensive research (e.g., [Meyer & Stroyer-Hansen 1972](#); [McCarthy et al. 2004a,b](#); [Thorwirth et al. 2005](#)). Figure 1 shows the most stable structures and their electronic states found with our computational methodology. In the following, we provide a comparison between our results and literature data. Singlet and triplet state energies of each species can be found in Appendix A.

In their quantum chemical investigation, [Raghavachari et al. \(1990\)](#) showed that the most stable conformation for S_3 was a chain, in a singlet electronic state. Our calculations agree with this hypothesis, when an open-shell singlet electronic configuration is assumed. Moreover, we found that the second most stable configuration is the closed shell singlet spin state, closely followed by a ring structure with a closed-shell singlet electronic state.

For S_4 , DFT calculations have revealed six possible isomers, involving both chains and rings, which can be detected under non-equilibrium conditions ([Eckert & Steudel 2003](#)).

The open chain structure with C_{2v} symmetry and an open-shell singlet electronic state was reported as the most stable isomer ([McCarthy et al. 2004b](#)), which is in agreement with our calculations at BHYLP-D3(BJ) level of theory.

S_5 is a minority species in sulfur vapor at all temperatures and pressures ([Steudel et al. 2003](#)), and is the least characterized structure, for which no spectral information is available. Only one minimum can be found on the PES of S_5 , corresponding to the envelope conformation, while the half-chair conformation is a saddle point ([Cioslowski et al. 2001](#)). In our calculations, we find that the energy difference between the two conformations is 0.7 kJ mol⁻¹ at DFT level of theory, and the presence of an imaginary frequency for the half-chair conformation confirms that the envelope structure is the correct minimum.

Rings as S_6 and larger can also be found in the solid phase. S_6 is a highly symmetric homocycle, the most stable conformer being the chair conformation, in anal-

ogy to cyclohexane. S_7 is better known for existing in four bulk allotropic forms, while a ring with C_s symmetry is the favored conformer in the gas phase. S_8 constitutes the most thermodynamically stable and thus the common form of sulfur, and has been determined to adopt a crown-shaped geometry in the gas phase (Raghavachari et al. 1990).

In summary, the ground states of the species targeted in this study are open-shell triplet for S and S_2 , open-shell singlet for the chains S_3 and S_4 , and closed-shell singlet for the rings from S_5 to S_8 , all in agreement with previous literature data.

3.2. S_n /ice adsorption complexes and BEs

For each S_n species, we considered two adsorption complexes on the amorphous ice model, initially locating the species on regions either geometrically flat or in the small surface cavity (highlighted by the target icon in Figure 1). Table 1 reports the computed BE(0) values and Figure 2 plots a comparative trend of the BE(0)s when the S_n species are adsorbed in either the cavity or on the flat regions. The terms contributing to the BE(0) values are reported in Table 2.

The interaction between the S_n species and the ice is almost entirely due to: i) electronic effects (contributed by electrostatic interaction, Pauli repulsion and orbital interaction due to charge transfer and polarization effects), and ii) London dispersion interactions. The percentage of the dispersion interactions contribution to each BE value (see Table 2) shows their dominance, with the exception of atomic sulfur, for which 40% to 50% of the ΔE is due to the electronic contribution. For S_2 and S_4 cases, dispersion interactions even compensate for the slight repulsion from the pure electronic interactions ΔE . Therefore, the binding energy is dominated by dispersion interactions, which are governed by the mutual polarizability of the interacting species (ice grain and the S_n species). Indeed, S_n species exhibit a highly polarizability but negligible electric multipoles providing small contribution to the electrostatic component of the BE. For the same reasons, also the charge transfer contribution is very small. Accordingly, we obtain dispersion contributions ranging 70–100% of the total binding energy.

The BE(0) values reported in Table 1 indicate that S and S_2 are the two S-bearing species with the lower BE(0)s, obviously due to the more limited electronic and dispersion contributions. Remarkably, in the cavity region, atomic S interacts more strongly than S_2 , as occurs for H and O compared to their corresponding (more inert and stable) diatomic H_2 and O_2 species (Ferrero et al. 2020a,b; Minissale et al. 2022). From S_2 to S_8 ,

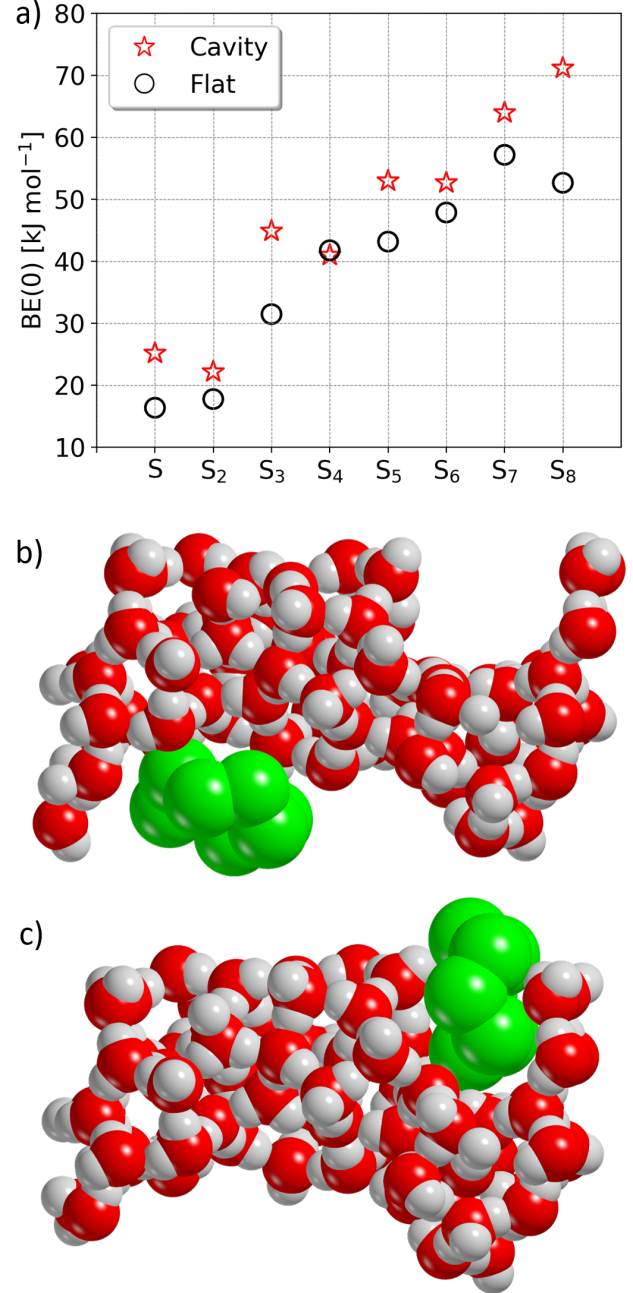


Figure 2. a) Binding energies (BE(0), in kJ mol^{-1}) of S-chains at BHLYP-D3(BJ)/A-VTZ* level of theory adsorbed onto the amorphous model (cavity site, star; flat site, circle). Adsorption geometries of S_8 onto the amorphous ice surface: b) flat region; c) cavity region.

the BE(0)s (and in particular the ΔE^* term, free from the deformation energies, see Table 2) increases with the number of S atoms, as each atomic S addition gives further interactions in the S_n /ice complexes. That is, although dispersion forces are weak, the sum of several small contributions can result in large interaction en-

ergies, especially when the adsorbate has several atoms due to establishing a large contact area with the surface. This effect is responsible for the increase of the BE with the number of S atoms in the adsorbed species, even in the absence of local interactions such as the hydrogen bonds.

The morphology of the surface binding site affects the resulting BE(0). Indeed, in most cases, the BE(0) in the cavity region is larger than that on the flat region (see panel a) of Figure 2). There is a good fit between the two sets of BE(0)s revealing an increase of about 18% of the BE(0) when passing from flat to the cavity regions. As outlined before, the dispersion forces, responsible of the S_n /ice interactions, strongly depend on the contact area between the adsorbates and the surface water molecules, becoming larger for larger surface contact due to the higher polarizability effects onto the S_n species. In the amorphous cavity regions, almost every S atom of the adsorbed species interacts with the surface water molecules, while on the flat region, only some atoms of the adsorbate are directly facing the water molecules of the surface, the rest being oriented toward the gas phase. This results in a higher weight of dispersion interactions for species adsorbed in the cavity region (see panels b and c of Figure 2). The only exception is S_4 (with similar BE(0)s for the two regions), because the interaction of S_4 with the cavity is associated with a large deformation of the cavity surface region (listed in Table 2).

The adsorption of large rings in the cavity means, to some extent, a structural rearrangement of the surface to fit the molecule in the cavity. This is reflected by the increment of the surface deformation energy (δE_S) with the increase of the number of S atoms, in particular for the S_7 and S_8 cases. In contrast, the deformation of the adsorbed species (δE_μ) is of few kJ mol^{-1} , since they do not suffer from structural modifications due to their weak interactions with the ice.

The lateral interaction energy (δE_L) between adsorbates in adjacent cells (whose absolute value is mainly below 2 kJ mol^{-1} , see Table 2), is indicative of the adequate dimensions of the unit cells for the simulation of the freeze-out of an isolated S_n species.

In the literature, the only previous study on the BEs of species from S_3 to S_8 is based on an experimental work by Cazaux et al. (2022) (see Table 1). The BEs of S_2 – S_4 are estimated from temperature programmed desorption (TPD) experiments, based on the empirical rule defined in Luna et al. (2017), while the BEs of S_5 – S_8 are extrapolated based on the trend obtained for S_2 – S_4 . However, the species were formed by H_2S photoprocessing, and therefore, their BE data are not relative to the adsorp-

tion on water ice, but rather the result of self interactions among the different sulfur species formed during the experiment. For this reason, the comparison between the BEs computed in this work and those estimated and/or extrapolated in Cazaux et al. (2022) is not straightforward. A new set of experiments performed on water ice would be necessary to compare the data obtained from our calculations. From our own computed data, we plotted the average binding energy of each species, $\text{BE}(0)_{avg} = (\text{BE}(0)_{cavity} + \text{BE}(0)_{flat})/2$, against the number of S atoms of the adsorbate (see Fig. 3). Clearly, the increase in BE(0)s with the number of S atoms does not simply scale linearly. Rather, it seems that close couples (S_1 – S_2 , S_3 – S_4 , S_5 – S_6 and S_7 – S_8) exhibit almost the same BE(0). Although the first increase between pairs is steep (20 kJ mol^{-1}), the others are more moderate (10 kJ mol^{-1}). This seems to be due to the same number of S atoms facing the ice surface (three S atoms for S_5 – S_6 , four S atoms for S_7 – S_8 cases), significantly changing the dispersive interactions. Even if quite rough for the above reasons, the linear best fit of Fig. 3 gives an increment of about 9 kJ mol^{-1} to the $\text{BE}(0)_{avg}$ for each added S atom. This increment is approximately half of the value proposed in the literature, which was set to 20 kJ mol^{-1} per S atom (see Cazaux et al. (2022)). Therefore, we would like to raise awareness about the magnitude of the BEs reported in the literature, as its use in astrochemical modeling has a significant impact on the desorption rates. To have deeper insights into this point (namely, the influence of an error in the BE on the desorption rate constant), we calculated the ratio between desorption rates, r_{des} with an error δ on the BE, that is:

$$r_{des} = \frac{k_{des}(\text{BE})}{k_{des}(\text{BE} + \delta)} = \exp\left(\frac{\delta}{RT}\right) \quad (2)$$

Note that r_{des} does not depend on the BE itself. Larger errors will have a major impact at low temperatures, while they will be smeared out at high temperatures, bringing the δ/RT term towards zero. Considering the limit of chemical accuracy, the error is $\delta = 4 \text{ kJ mol}^{-1}$, meaning that at $T = 10 \text{ K}$ such error implies a difference of 20 orders of magnitude on the k_{des} . At such low temperatures, however, thermal desorption of sulfur allotropes is negligible and the impact of our estimations in the gas chemistry would be moderate. In contrast, thermal desorption can be dominant in warmer regions, around young protostars. In these environments, dust temperatures are $> 50 \text{ K}$ and some volatile compounds can be sublimated. At these temperatures, an error of $\delta = 4 \text{ kJ mol}^{-1}$ reduces the difference on the k_{des} to ~ 4 orders of magnitude, with a significant impact in the

Table 1. BE(0) in kJ mol^{-1} for S_n species adsorbed on the two binding regions of the amorphous ice model, computed at BLYP-D3(BJ)/A-VTZ* level of theory. Values from the literature are listed for comparison.

BE(0)	Surface	S	S_2	S_3	S_4	S_5	S_6	S_7	S_8
Flat (this work)	Comput., periodic H_2O ice	16.4	17.8	31.5	41.8	43.2	47.9	57.5	52.7
Cavity (this work)	Comput., periodic H_2O ice	25.5	22.2	44.9	41.0	53.0	52.7	64.0	71.2
Perrero et al. (2022)	Comput., periodic H_2O ice	13.1-23.3	8.6-20.4						
Cazaux et al. (2022)	Exp., H_2S ice		28.2 ^a	49.9 ^a	70.6 ^a	89.8 ^b	109.7 ^b	129.7 ^b	149.7 ^b
Penteado et al. (2017)	Exp. & Comput.	8.2 ± 4.1	16.6 ± 4.1						
Wakelam et al. (2017)	Comput., 1 H_2O		21.6						
Das et al. (2018)	Comput., $(\text{H}_2\text{O})_4$ cluster	11.9		13.7					
KIDA (Wakelam et al. 2015)	—	21.6 ^c		18.3 ^d					
UMIST (McElroy et al. 2013)	—	9.1 ^d		18.3 ^d					

^aValues derived from laboratory experiments. ^bExtrapolated values (see text for details).

^cValue from Wakelam et al. (2017). ^dValues from Hasegawa et al. (1992).

abundances of these species in gas phase. Thus, the impact of minor inaccuracies in the BE on the results of a chemical model depends on the specific conditions of the region under study. The same absolute error on different BE values will have the same impact on the desorption rate, in which such an impact depends in turn on the considered environment.

tle, while Das et al. (2018) used a water tetramer as ice analogue for studying S and S_2 adsorptions. An estimate of the BE of S and S_2 was provided by Penteado et al. (2017), in a review collecting values from both theoretical and experimental works. Other values of the BEs are tabulated in UMIST and KIDA databases (McElroy et al. 2013; Wakelam et al. 2015). We also contributed, in a recent work (Perrero et al. 2022), to the BEs of S and S_2 , while giving a range of BEs (computed at the M062X-D3/A-VTZ*//HF-3c level of theory) for each species on eight different binding sites available in the amorphous ice model of this work. Interestingly, the BEs computed in the present work for S and S_2 , cover the upper and lower limits of the ranges provided in Perrero et al. (2022). The computed BEs of S_2 were in agreement with previous literature values, while for atomic S the weakest tail of the calculated BE range did not include the even smaller values proposed by (Penteado et al. 2017) and by the UMIST database (McElroy et al. 2013). All the BE values reported in the literature are collected in Table 1.

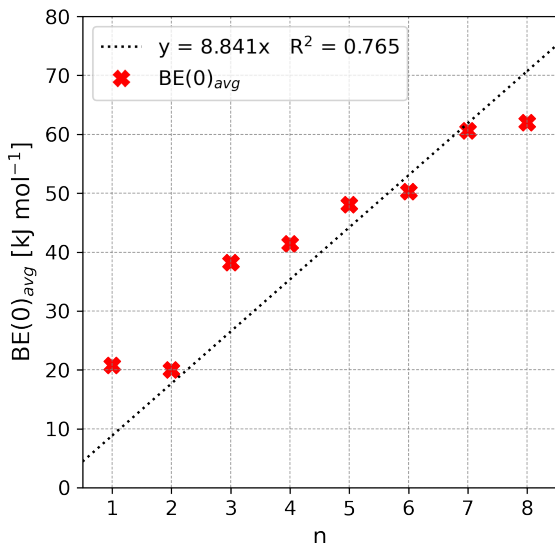


Figure 3. Correlation between the $\text{BE}(0)_{\text{avg}}$ and the number n of atoms of each S_n species. The linear fit does not seem appropriate to define the trend, as it appears that the increase of $\text{BE}(0)$ happens in steps every couple of species.

As for atomic S and S_2 molecule, *ab initio* literature calculations have been performed to compute their BEs on interstellar ice mantles. For atomic S, Wakelam et al. (2017) used one water molecule to simulate the ice man-

3.3. Vibrational spectroscopic features

Here, we focus on the calculation of the frequencies (ν) of the S_n species (for $n=2-8$) as gas-phase and as adsorbed complexes, for IR and Raman spectra. Table 3 shows the whole set of computed vibrational frequencies for the considered cases, while Figure 4 shows the comparison between the largest S_8 molecules in gas-phase and when adsorbed on the flat region.

Several studies have measured experimentally or simulated theoretically the spectra of these species, both in the gas phase or in the condensed phase. The reviews of Eckert & Steudel (2003) and Trofimov et al. (2009) are particularly useful for gathering detailed information. The main vibrational features available in the literature

Table 2. Contributions to the BE(0)s (in kJ mol^{-1}) of the adsorption complexes modeled on the flat region and in the cavity region of the amorphous ice model, computed at BLYP-D3(BJ)/A-VTZ* level of theory. The equations showing how the terms add up are reported and explained in the Appendix B. ΔE is the bare interaction energy, splitted in the electronic ΔE_{elect} and dispersive contributions ΔE_{disp} , the latter also in percentage; δE_S is the deformation energy of the surface; δE_μ is the deformation energy of the adsorbate; δE_L is the lateral interaction energy; ΔE^* is the deformation-free interaction energy; and the BSSE is the basis set superposition error.

Flat Region	S	S_2	S_3	S_4	S_5	S_6	S_7	S_8
ΔE	-18.3	-23.3	-39.3	-53.0	-50.9	-60.2	-68.0	-63.7
ΔE_{elect}	-7.1	+0.5	-9.4	+0.9	-20.1	-1.4	-12.1	-8.7
ΔE_{disp} (%)	-11.2 (61)	-23.8 (102)	-29.9 (76)	-54.0 (102)	-30.9 (61)	-58.8 (98)	-55.9 (82)	-55.0 (86)
δE_S	0.7	0.9	5.1	3.0	5.2	13.7	4.7	3.8
δE_μ	0.0	0.3	3.3	9.0	0.5	0.5	0.4	1.2
δE_L	0.0	-0.3	-0.1	-0.1	-0.4	-0.6	-1.0	-1.5
ΔE^*	-19.0	-24.2	-47.6	-65.0	-56.1	-73.8	-72.1	-67.2
BSSE	-1.9	-4.3	-6.0	-8.9	-5.8	-10.5	-8.5	-9.5
Cavity Region	S	S_2	S_3	S_4	S_5	S_6	S_7	S_8
ΔE	-27.6	-28.3	-53.8	-51.5	-63.4	-64.6	-78.3	-87.7
ΔE_{elect}	-14.0	+1.7	-15.2	+0.8	-11.3	+0.9	-6.3	-2.8
ΔE_{disp} (%)	-13.6 (49)	-30.0 (106)	-38.7 (66)	-52.3 (102)	-52.1 (82)	-65.5 (101)	-72.0 (92)	-85.0 (97)
δE_S	5.0	1.6	2.3	10.7	8.3	6.4	10.3	9.7
δE_μ	0.0	0.0	0.0	0.0	0.6	0.3	0.4	0.7
δE_L	0.0	0.0	-0.1	-0.3	-0.4	-0.4	-0.7	-1.4
ΔE^*	-32.7	-29.9	-56.0	-62.0	-71.9	-70.9	-88.3	-96.8
BSSE	-2.4	-4.8	-6.9	-8.7	-8.4	-10.3	-12.2	-14.7

are reported in Table 3. It is worth noting that the comparison between the frequencies reported in the literature and those computed in this work is not always satisfying. For example, Lenain et al. (1988) reports a stretching vibration for S_2 of 715 cm^{-1} , while our calculations give a value of 747 cm^{-1} . For S_3 , Brabson et al. (1991) and Picquenard et al. (1993) give 281 cm^{-1} (Raman) for the bending, and 581 cm^{-1} (Raman) and 680 (IR) cm^{-1} for the symmetric and antisymmetric stretching, respectively, while we find values of 254, 520 and 639 cm^{-1} . We can immediately see that the differences are large, even considering that highly accurate quantum-chemical calculations have been performed, in agreement with what is reported in the literature (Steudel et al. 2003).

It is worth noting that no scaling was applied to our computed frequencies. Nevertheless, the absolute prediction of the vibrational frequencies is not the focus of this work; we are rather interested in highlighting the frequency shifts of the S_n species vibrational modes with respect to the gas-phase values due to their interaction with the ice.

As mentioned above, the interaction between the S_n species and the water ice surfaces is almost totally governed by London dispersion forces, which are

very weak forces based on permanent dipole – induced dipole moments, and therefore are non-specific and non-directional (at variance with the H-bonding). In our case, the dispersion contribution arises from the interaction between the permanent dipole moment of the water surface molecules and the temporary or induced dipoles of the S_n adsorbates. The fact that dispersion forces are non-specific and do not establish vibrational coupling with the water surface causes the adsorption of S_n species to be either only slightly perturbed or to have a null affect to the vibrational modes of the adsorbates. Consequently, the infrared spectra are almost unperturbed with respect to the free S_n species. Additionally, the shifts observed when comparing gas-phase and adsorbed species vibrational features further decrease with the molecular size of the adsorbate. This is in agreement with the decreasing contribution of the electronic component of the BE(0) with the molecular size and the increasing role of the non-specific London type interactions. In general, we notice that both IR and Raman peaks suffer a small hypsochromic shift, due to a slight increase in the bond strength. We notice such an effect on S_3 , whose bond lengths change from 1.951 \AA in the gas phase to 1.901 \AA and 1.930 \AA for the adsorbed molecule on the flat and cavity region of the ice. Such

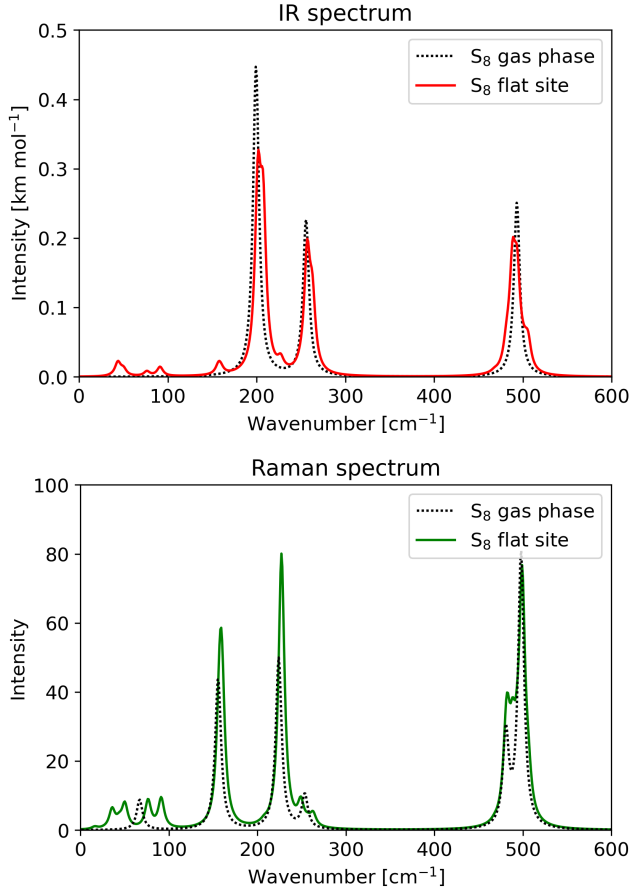


Figure 4. IR and Raman spectra of S_8 computed at BHLYP-D3(BJ)/A-VTZ* level of theory. Dotted lines: gas-phase species. Solid lines: adsorbed species. IR intensities are in km mol^{-1} , while Raman intensities are given in arbitrary units.

variations correspond to a hypsochromic shift of $\Delta\nu = 70 \text{ cm}^{-1}$ on the asymmetric stretching vibration (the only active IR mode). However, such a strong variation is observed only for S_3 (and S_4 , see below), while for the other species the caused change is much smaller (about $\Delta\nu = 0\text{--}10 \text{ cm}^{-1}$). S_2 experiences no shift due to adsorption, as evidenced by the unaltered bond length (1.899 Å) and is consistent with its weak interaction with ice. While the S_2 stretching peak is active in Raman spectroscopy, in the IR spectra it is possible to distinguish between the gas-phase and the adsorbed cases. For symmetry, no bands are observed in the gas-phase, while the interaction with the ice slightly activates this mode. The same phenomenon has been documented for CH_4 and NH_4SH , whose IR spectral features are affected by the presence of an amorphous water ice matrix interacting with the adsorbate (Escribano et al. 2014; Hudson et al. 2015). Finally, for S_4 , an interesting aspect appears: while there is no significant difference between

the gas-phase and on the cavity region spectra, this is juxtaposed by a large change in the vibrational features on the flat region. That is, $\Delta\nu$ of the first two bending modes is $20\text{--}30 \text{ cm}^{-1}$, and $\Delta\nu > 100 \text{ cm}^{-1}$ for the third vibrational mode. The explanation can be found in the geometrical features of the molecule: for all the cases (gas-phase and on both ice regions) the optimized conformer of S_4 falls into the C_{2v} symmetry. The gas-phase S-S bond length of 2.201 Å shorten to 2.193 Å when adsorbed on the cavity, with a corresponding hypsochromic shift of $\Delta\nu = 20\text{--}30 \text{ cm}^{-1}$. Even more so, when adsorbed on the flat region, the S-S bond length decreases to 2.056 Å, with a large hypsochromic shift of its stretching frequency ($\Delta\nu > 100 \text{ cm}^{-1}$).

In principle the present outcome may guide the interpretation of the JWST spectra detection of interstellar ice, at least for what concerns the IR spectra. However, the absolute intensity of each IR vibrational mode is an important parameter as it regulates the chance of being observed. Our results show many IR peaks with almost negligible intensities (which become smaller as the length of the S-chain increases), as the dipole changes during vibration are almost negligible for the homo-nuclear S_n rings. It is a pity that Raman spectra of the interstellar matter cannot, unfortunately, be observed with the present technology as the Raman intensities, depending on the polarizability of the molecule, are rather high. Indeed, sulfur is a large and easily polarizable atom, imparting high polarizability to the S_n species. For the time being, Raman can be adopted in terrestrial experiments of the kind reported by Cazaux et al. (2022) to characterize the S-bearing species.

Ices in interstellar environments are primarily identified by their vibrational transitions in the near-to-far IR. In general, the $1\text{--}3 \mu\text{m}$ wavelength region contains combination and overtone modes, the $3\text{--}6 \mu\text{m}$ region comprehends the stretching vibrations, the $6\text{--}30 \mu\text{m}$ region the bending and libration vibrations, while the $25\text{--}300 \mu\text{m}$ region represents torsional and intermolecular (lattice) modes (Boogert et al. 2015).

The frequencies covered by the vibrational modes of the investigated S_n species span the $150\text{--}750 \text{ cm}^{-1}$ range, corresponding to a wavelength range of $13.3\text{--}66.6 \mu\text{m}$. Above $30 \mu\text{m}$ the availability and capability of instrumentation are limited, e.g. the JWST is designed to observe in the wavelength range from 0.6 to $27 \mu\text{m}$ (Rauscher & Ressler 2005). In addition, both amorphous and crystalline olivine and forsterite exhibit bending and torsional modes within the $14\text{--}24 \mu\text{m}$ region (Zamirri et al. 2019; Boogert et al. 2015), and libration modes of water cover the region around $10\text{--}12 \mu\text{m}$ (Gibb et al. 2000; McClure et al. 2023).

Therefore, the forest of vibrational bands located in that region of the spectra, along with the weak intensities of the vibrational S_n peaks, may render their IR detection rather difficult. When moving to terrestrial laboratory experiments, the seminal work of [Anderson & Loh \(1969\)](#) suggested that Raman spectroscopy is ideal for the characterization of sulfur allotropes, due to the ability to distinguish and assign several active vibration modes, as also shown in Table 3 from the computed ones. Thus, Raman bands simulated here can serve as proxies for the detection of the S_n species adsorbed on the ices in terrestrial laboratory experiments. This would be the case, for instance, of the stretching modes around 500 cm^{-1} , which are all active in Raman while invisible in IR.

4. CONCLUSIONS

In this work, we computed the zero point corrected binding energies (BE(0)s) and the vibrational features (both IR and Raman spectra inclusive of absolute intensities) of the adsorption complexes of S_n species ($n=1-8$) on an amorphous water ice surface model by means of quantum chemical simulations. The ice model was already proposed by some of us [Ferrero et al. \(2020b\)](#); [Perrero et al. \(2022\)](#) to study the interaction of many different molecules of astrochemical interest.

We adopted *ab initio* periodic calculations based on the BHLYP-D3(BJ)/A-VTZ* model chemistry for both the geometry optimization and the computation of IR and Raman spectra in the harmonic approximation (for frequencies and intensities). To simplify the modeling due to the large size of the S_n species, we focused on two different regions of the amorphous ice model. The first exhibits a cavity, mimicking some ice porosity in which the contact between the adsorbate and the ice surface is at its maximum. The second is a flat region, which represents a portion of dense icy dust grains. This limits the number of BEs (mainly two) that we obtain, but we expect these values to well represent the upper and lower limits of the range that one would obtain by conducting a broader sampling of binding sites. The BE(0)s of the S_n species resulted about 18% higher for the cavity region than for the flat one, as expected due to the non-specific nature of the interactions. These two situations likely represent the tail limits of a complete BE(0)s distribution that can be computed on much larger (and not feasible with our computational facilities) icy grain models. Currently, a few chemical models exist where more than one BE value for each species can be included. Moreover, several works are focusing on the computation of BEs distribution histograms, e.g., [Bovolenta et al. \(2022\)](#); [Tinacci et al. \(2022, 2023\)](#), as more representa-

tive of the variety of binding sites that a real amorphous ice mantle could offer. A distribution of values with a statistical meaning allows determining a mean BE and a standard deviation for each species. However, if we were to suggest a single BE value to be adopted in chemical models, the average between the two BEs computed for each species should be a reasonable choice. Nonetheless, we are aware that a more meticulous sampling of the ice model would be necessary in order to provide statistically meaningful data.

We found that the BE(0) values of the S_n species increase with the number of S atoms, and that their interaction with the ice is mainly driven by dispersion-like (London) interactions. Only for the single S atom, a major electronic effect contribution was detected. We found only a rough linear correlation between the averaged BE(0) values of the two surface regions and the number of sulfur atoms, with an increment by each S atom of about 9 kJ/mol , which may be useful to guess the BE(0) for even larger sulfur polymorphs by simple addition. A deeper analysis revealed that close couples (S_1-S_2 , S_3-S_4 , S_5-S_6 and S_7-S_8) exhibit almost the same BE(0). From the analysis of the IR and Raman spectra, it is not possible to easily distinguish between gas-phase and adsorbed species, given that the perturbations suffered by the vibrational features of the adsorbed species are small and, overall, their amount becomes smaller with the increasing size of the S_n species. Thus, the species exhibiting significative vibrational frequency perturbations upon adsorption are S_n with $n=2-4$. The intensities of the IR and Raman peaks suggest Raman spectroscopy (due to the large polarizability of sulfur and its allotropic forms) to be the technique of election for the detection of S_n species in terrestrial laboratory experiments as Raman cannot, unfortunately, be used for studying the ISM spectral features.

5. ACKNOWLEDGMENTS

This project has received funding within the European Union’s Horizon 2020 research and innovation programme from the European Research Council (ERC) for the projects “Quantum Chemistry on Interstellar Grains” (QUANTUMGRAIN), grant agreement No. 865657, and “The trail of sulfur: from molecular clouds to life” (SUL4LIFE), grant agreement No. 101096293. The Italian Space Agency for co-funding the Life in Space Project (ASI N. 2019-3-U.O), the Italian MUR (PRIN 2020, Astrochemistry beyond the second period elements, Prot. 2020AFB3FX) are also acknowledged for financial support. Authors (J.P. and P.U.) acknowledge support from the Project CH4.0 under the MUR program “Dipartimenti di Ec-

Table 3. Vibrational frequencies in cm^{-1} computed at full BHLYP-D3(BJ)/A-VTZ* level. The first seven row are dedicated to computed values, while the last three column are dedicated to literature values. The second row reports the frequencies computed for the gas-phase molecule, while the third and the fourth columns report the ones of the adsorbate in the cavity and on the flat region of the amorphous model. The peaks are classified as stretching (S), bending (B), and other (O, representing different types of torsion), and it is indicated if they are IR or Raman active. The literature values are taken from [Eckert & Steudel \(2003\)](#) with the exception of S_4 , for which we refer to the work of [Picquenard et al. \(1993\)](#)^(a). For the sake of clarity, only strong bands for each species are reported. Origin of the spectra: S_2 was recorded in the gas phase; S_3 from sulfur vapors and matrix isolation in solid argon; S_4 in saturated and unsaturated sulfur vapor; solid S_6 , $\alpha\text{-S}_7$, and $\alpha\text{-S}_8$ were used to record their spectra. For a complete list of all the features, we refer the reader to [Eckert & Steudel \(2003\)](#) and [Trofimov et al. \(2009\)](#).

Specie	Gas-phase	Cavity Region	Flat Region	Type	IR	Raman	Tabulated Freq	Type	Source
S_2	747	745	746	S		X	715	S	Raman
S_3	254	267	264	B		X	281	B	Raman
	520	518	556	S		X	581	S sym	Raman
	639	643	711	S	X	X	680	S antisym	IR
S_4	140	151	171	B		X			
	310	315	330	B		X	303 ^a	B	Raman
	322	336	458	B	X	X			
	656	655	669	S	X		575 ^a	S	Raman
	662	665	670/681	S		X	680 ^a /683	S	Raman/IR
S_5	245	254	253	O	X	X			
	306	308	307	B	X	X			
	416	426/436	427	S		X			
	423	426	423	S	X				
	460	467	466	S	X	X			
	525	516	524	S	X				
S_6	528	516/535	524	S		X			
	167	175	176	O	X		180	O	IR
	215	219	219	O	X(no gas)	X			
	274	278	277	O		X			
	329	333	333	O	X		313	B	IR
	-	441	444	S	X				
	486	490	490	S	X	X	463	S	IR
S_7	504	505	504	S		X			
	160	169	165	O		X			
	181	186	187	O	X(no gas)	X			
	243	251	247	B	X	X	235	B	IR
	285	290	288	B	X		270	B	IR
	300	298	303	B		X			
	411	410	409	S	X	X	400	S	IR
	451	464	459	S	X	X	480	S	IR
	506	504	507	S	X	X	513	S	IR
S_8	536	527	526	S		X			
							90	O	IR/Raman
	155	162	159	B		X	150-250	B	IR/Raman
	199	207	202	O	X				
	224	230	227	O		X			
	253	255	249	O		X			
	256	261	257	O	X				
	481	488	482	S		X	410-480	S	IR/Raman
	493	494	489	S	X				
	498	501	499	S		X			

celenza 2023-2027" (CUP: D13C22003520001). The Spanish MICINN is also acknowledged for funding the projects PID2021-126427NB-I00 (A.R.), PID2019-106235GB-I00 (A.F.), PID2020-116726RB-I00 (L.B.-A.), and CNS2023-144902 (A.R.). The authors thankfully acknowledge RES resources provided by BSC in MareNostrum to activities QHS-2022-3-0007 and QHS-

2023-2-0011, and the supercomputational facilities provided by CSUC.

Supplementary Material consisting of (i) the fractional coordinates of DFT adsorption structures optimized for the amorphous ice models, and (ii) images of the computed IR and Raman spectra, is available at <https://zenodo.org/records/10650677>.

REFERENCES

- Altwegg, K., Combi, M., Fuselier, S. A., et al. 2022, *MNRAS*, 516, 3900, doi: [10.1093/mnras/stac2440](https://doi.org/10.1093/mnras/stac2440)
- Anderson, A., & Loh, Y. T. 1969, *Can. J. Chem.*, 47, 879, doi: [10.1139/v69-145](https://doi.org/10.1139/v69-145)
- Aponte, J. C., Dworkin, J. P., Glavin, D. P., et al. 2023, *EPS*, 75, 28, doi: [10.1186/s40623-022-01758-4](https://doi.org/10.1186/s40623-022-01758-4)
- Becke, A. D. 1993, *J. Chem. Phys.*, 98, 1372, doi: [10.1063/1.464304](https://doi.org/10.1063/1.464304)
- Boogert, A., Brewer, K., Brittain, A., & Emerson, K. 2022, *ApJ*, 941, 32, doi: [10.3847/1538-4357/ac9b4a](https://doi.org/10.3847/1538-4357/ac9b4a)
- Boogert, A. A., Gerakines, P. A., & Whittet, D. C. 2015, *ARA&A*, 53, 541, doi: [10.1146/annurev-astro-082214-122348](https://doi.org/10.1146/annurev-astro-082214-122348)
- Bovolenta, G. M., Vogt-Geisse, S., Bovino, S., & Grassi, T. 2022, *ApJS*, 262, 17, doi: [10.3847/1538-4365/ac7f31](https://doi.org/10.3847/1538-4365/ac7f31)
- Brabson, G. D., Mielke, Z., & Andrews, L. 1991, *J. Phys. Chem.*, 95, 79, doi: [10.1021/j100154a019](https://doi.org/10.1021/j100154a019)
- Calmonte, U., Altwegg, K., Balsiger, H., et al. 2016, *MNRAS*, 462, S253, doi: [10.1093/mnras/stw2601](https://doi.org/10.1093/mnras/stw2601)
- Caselli, P., Hasegawa, T., & Herbst, E. 1994, *ApJ*, 421, 206, doi: [10.1086/173637](https://doi.org/10.1086/173637)
- Cazaux, S., Carrascosa, H., Caro, G. M., et al. 2022, *A&A*, 657, A100, doi: [10.1051/0004-6361/202141861](https://doi.org/10.1051/0004-6361/202141861)
- Cioslowski, J., Szarecka, A., & Moncrieff, D. 2001, *J. Phys. Chem. A*, 105, 501, doi: [10.1021/jp003339g](https://doi.org/10.1021/jp003339g)
- Das, A., Sil, M., Gorai, P., Chakrabarti, S. K., & Loison, J. C. 2018, *ApJS*, 237, 9, doi: [10.3847/1538-4365/aac886](https://doi.org/10.3847/1538-4365/aac886)
- Dovesi, R., Erba, A., Orlando, R., et al. 2018, *WIREs Comput. Mol. Sci.*, 8, e1360, doi: [10.1002/wcms.1360](https://doi.org/10.1002/wcms.1360)
- Eckert, B., & Steudel, R. 2003, *Molecular Spectra of Sulfur Molecules and Solid Sulfur Allotropes*, ed. R. Steudel (Berlin, Heidelberg: Springer Berlin Heidelberg), 31–98, doi: [10.1007/b13181](https://doi.org/10.1007/b13181)
- Escribano, R., Timón, V., Gálvez, O., et al. 2014, *Phys. Chem. Chem. Phys.*, 16, 16694, doi: [10.1039/C4CP01573H](https://doi.org/10.1039/C4CP01573H)
- Ferrante, R. F., Moore, M. H., Spiliotis, M. M., & Hudson, R. L. 2008, *ApJ*, 684, 1210, doi: [10.1086/590362](https://doi.org/10.1086/590362)
- Ferrero, S., Martínez-Bachs, B., Enrique-Romero, J., & Rimola, A. 2020a, in *Computational Science and Its Applications – ICCSA 2020*, ed. O. Gervasi, B. Murgante, S. Misra, C. Garau, I. Blečić, D. Taniar, B. O. Apduhan, A. M. A. C. Rocha, E. Tarantino, C. M. Torre, & Y. Karaca (Cham: Springer International Publishing), 553–560, doi: [10.1007/978-3-030-58814-4_41](https://doi.org/10.1007/978-3-030-58814-4_41)
- Ferrero, S., Zamirri, L., Ceccarelli, C., et al. 2020b, *ApJ*, 904, 11, doi: [10.3847/1538-4357/abb953](https://doi.org/10.3847/1538-4357/abb953)
- Fuente, A., Goicoechea, J. R., Pety, J., et al. 2017, *ApJL*, 851, L49, doi: [10.3847/2041-8213/aaa01b](https://doi.org/10.3847/2041-8213/aaa01b)
- Fuente, A., Rivière-Marichalar, P., Beitia-Antero, L., et al. 2023, *A&A*, 670, A114, doi: [10.1051/0004-6361/202244843](https://doi.org/10.1051/0004-6361/202244843)
- Gibb, E. L., Whittet, D. C. B., Schutte, W. A., et al. 2000, *ApJ*, 536, 347, doi: [10.1086/308940](https://doi.org/10.1086/308940)
- Gondhalekar, P. M. 1985, *MNRAS*, 217, 585, doi: [10.1093/mnras/217.3.585](https://doi.org/10.1093/mnras/217.3.585)
- Grimme, S., Antony, J., Ehrlich, S., & Krieg, H. 2010, *J. Chem. Phys.*, 132, 154104, doi: [10.1063/1.3382344](https://doi.org/10.1063/1.3382344)
- Hasegawa, T. I., Herbst, E., & Leung, C. M. 1992, *ApJS*, 82, 167, doi: [10.1086/191713](https://doi.org/10.1086/191713)
- Hudson, R. L., Gerakines, P. A., & Loeffler, M. J. 2015, *Phys. Chem. Chem. Phys.*, 17, 12545, doi: [10.1039/C5CP00975H](https://doi.org/10.1039/C5CP00975H)
- Jenkins, E. B. 2009, *ApJ*, 700, 1299, doi: [10.1088/0004-637X/700/2/1299](https://doi.org/10.1088/0004-637X/700/2/1299)
- Jiménez-Escobar, A., & Caro, G. M. 2011, *A&A*, 536, A91, doi: [10.1051/0004-6361/201014821](https://doi.org/10.1051/0004-6361/201014821)
- Jiménez-Escobar, A., Muñoz Caro, G. M., & Chen, Y. J. 2014, *MNRAS*, 443, 343, doi: [10.1093/mnras/stu1100](https://doi.org/10.1093/mnras/stu1100)
- Laas, J. C., & Caselli, P. 2019, *A&A*, 624, A108, doi: [10.1051/0004-6361/201834446](https://doi.org/10.1051/0004-6361/201834446)
- Lee, C., Yang, W., & Parr, R. G. 1988, *Phys. Rev. B*, 37, 785, doi: [10.1103/PhysRevB.37.785](https://doi.org/10.1103/PhysRevB.37.785)
- Lenain, P., Picquenard, E., Corset, J., Jensen, D., & Steudel, R. 1988, *Berichte der Bunsengesellschaft für physikalische Chemie*, 92, 859, doi: [10.1002/bbpc.198800210](https://doi.org/10.1002/bbpc.198800210)

- Luna, R., Luna-Ferrández, R., Millán, C., et al. 2017, *ApJ*, 842, 51, doi: [10.3847/1538-4357/aa7562](https://doi.org/10.3847/1538-4357/aa7562)
- Maschio, L., Kirtman, B., Rérat, M., Orlando, R., & Dovesi, R. 2013a, *J. Chem. Phys.*, 139, 164101, doi: [10.1063/1.4824442](https://doi.org/10.1063/1.4824442)
- . 2013b, *J. Chem. Phys.*, 139, 164102, doi: [10.1063/1.4824443](https://doi.org/10.1063/1.4824443)
- McCarthy, M. C., Thorwirth, S., Gottlieb, C. A., & Thaddeus, P. 2004a, *Journal of the American Chemical Society*, 126, 4096, doi: [10.1021/ja049645f](https://doi.org/10.1021/ja049645f)
- . 2004b, *J. Chem. Phys.*, 121, 632, doi: [10.1063/1.1769372](https://doi.org/10.1063/1.1769372)
- McClure, M. K., Rocha, W. R. M., Pontoppidan, K. M., et al. 2023, *Nat. Astron.*, 7, 431–443, doi: [10.1038/s41550-022-01875-w](https://doi.org/10.1038/s41550-022-01875-w)
- McElroy, D., Walsh, C., Markwick, A. J., et al. 2013, *A&A*, 550, A36, doi: [10.1051/0004-6361/201220465](https://doi.org/10.1051/0004-6361/201220465)
- Meyer, B., & Stroyer-Hansen, T. 1972, *J. Phys. Chem.*, 76, 3968, doi: [10.1021/j100670a013](https://doi.org/10.1021/j100670a013)
- Minissale, M., Aikawa, Y., Bergin, E., et al. 2022, *ACS Earth Space Chem.*, 6, 597, doi: [10.1021/acsearthspacechem.1c00357](https://doi.org/10.1021/acsearthspacechem.1c00357)
- Pascale, F., Zicovich-Wilson, C. M., López Gejo, F., et al. 2004, *J. Comput. Chem.*, 25, 888, doi: [10.1002/jcc.20019](https://doi.org/10.1002/jcc.20019)
- Penteado, E. M., Walsh, C., & Cuppen, H. M. 2017, *ApJ*, 844, 71, doi: [10.3847/1538-4357/aa78f9](https://doi.org/10.3847/1538-4357/aa78f9)
- Perrero, J., Enrique-Romero, J., Ferrero, S., et al. 2022, *ApJ*, 938, 158, doi: [10.3847/1538-4357/ac9278](https://doi.org/10.3847/1538-4357/ac9278)
- Perrero, J., Ugliengo, P., Ceccarelli, C., & Rimola, A. 2023, *MNRAS*, 525, 2654, doi: [10.1093/mnras/stad2459](https://doi.org/10.1093/mnras/stad2459)
- Picquenard, E., Boumedien, M., & Corset, J. 1993, *J. Mol. Struct.*, 293, 63, doi: [10.1016/0022-2860\(93\)80015-N](https://doi.org/10.1016/0022-2860(93)80015-N)
- Raghavachari, K., Rohlfing, C. M., & Binkley, J. S. 1990, *J. Chem. Phys.*, 93, 5862, doi: [10.1063/1.459583](https://doi.org/10.1063/1.459583)
- Rauscher, B. J., & Ressler, M. E. 2005, *Experimental Astronomy*, 19, 149, doi: [10.1007/s10686-005-9015-0](https://doi.org/10.1007/s10686-005-9015-0)
- Ruffle, D. P., Hartquist, T. W., Caselli, P., & Williams, D. A. 1999, *MNRAS*, 306, 691, doi: [10.1046/j.1365-8711.1999.02562.x](https://doi.org/10.1046/j.1365-8711.1999.02562.x)
- Shingledecker, C. N., Lamberts, T., Laas, J. C., et al. 2020, *ApJ*, 888, 52, doi: [10.3847/1538-4357/ab5360](https://doi.org/10.3847/1538-4357/ab5360)
- Spitzer, L., & Jenkins, E. B. 1975, *ARA&A*, 13, 133, doi: [10.1146/annurev.aa.13.090175.001025](https://doi.org/10.1146/annurev.aa.13.090175.001025)
- Steudel, R., Steudel, Y., & Wong, M. W. 2003, *Speciation and Thermodynamics of Sulfur Vapor*, ed. R. Steudel (Berlin, Heidelberg: Springer Berlin Heidelberg), 117–134, doi: [10.1007/b12405](https://doi.org/10.1007/b12405)
- Thorwirth, S., McCarthy, M. C., Gottlieb, C. A., et al. 2005, *J. Chem. Phys.*, 123, 054326, doi: [10.1063/1.1942495](https://doi.org/10.1063/1.1942495)
- Tinacci, L., Germain, A., Pantaleone, S., et al. 2023, *ApJ*, 951, 32, doi: [10.3847/1538-4357/accae8](https://doi.org/10.3847/1538-4357/accae8)
- . 2022, *ACS Earth and Space Chemistry*, 6, 1514, doi: [10.1021/acsearthspacechem.2c00040](https://doi.org/10.1021/acsearthspacechem.2c00040)
- Trofimov, B., Sinegovskaya, L., & Guseva, N. 2009, *J. Sulfur Chem.*, 30, 518, doi: [10.1080/17415990902998579](https://doi.org/10.1080/17415990902998579)
- Wakelam, V., Castets, A., Ceccarelli, C., et al. 2004, *A&A*, 413, 609, doi: [10.1051/0004-6361:20031572](https://doi.org/10.1051/0004-6361:20031572)
- Wakelam, V., Loison, J.-C., Mereau, R., & Ruaud, M. 2017, *Mol. Astrophys.*, 6, 22, doi: [10.1016/j.molap.2017.01.002](https://doi.org/10.1016/j.molap.2017.01.002)
- Wakelam, V., Loison, J.-C., Herbst, E., et al. 2015, *ApJS*, 217, 20, doi: [10.1088/0067-0049/217/2/20](https://doi.org/10.1088/0067-0049/217/2/20)
- Zamirri, L., Macià Escatllar, A., Mariñoso Guiu, J., Ugliengo, P., & Bromley, S. T. 2019, *ACS Earth Space Chem.*, 3, 2323, doi: [10.1021/acsearthspacechem.9b00157](https://doi.org/10.1021/acsearthspacechem.9b00157)
- Zicovich-Wilson, C. M., Pascale, F., Roetti, C., et al. 2004, *J. Comput. Chem.*, 25, 1873, doi: [10.1002/jcc.20120](https://doi.org/10.1002/jcc.20120)

APPENDIX

A. S_N SPECIES DETAILS

We computed the energy gaps between different spin states of the S_n species characterized in this work. In the case of S and S_2 , their ground state is a triplet spin state. The singlet and the triplet spin states are well separated in energy (see Table A1).

Species	Closed Shell Singlet	Triplet
S	431	0
S_2	274	0

Table A1. Energy gaps (in kJ mol^{-1}) of atomic and diatomic sulphur species. The most stable structure is taken as the reference zero energy structure.

In contrast, S_3 , S_4 , and S_5 are more elusive and present electronic states closed in energy (see Table A2). The ground state of S_3 and S_4 is an open shell singlet. For S_3 the closed shell chain structure is only 10 kJ mol^{-1} less stable than the ground state, followed closely by the ring (in the close shell singlet state). In the case of S_4 , the second most stable configuration is the triplet spin state chain. The cyclic form of S_4 is the less favoured conformer. S_5 most stable conformed has a ring structure and a singlet ground state. This species has also been modeled as a chain, however, it is almost 70 kJ mol^{-1} less stable than the ring, when in the state of triplet or open shell singlet. The closed shell singlet configuration is remarkably unfavoured due to its planar geometry.

Finally, it is well established that S_6 , S_7 , and S_8 are ring structures with a closed shell singlet ground state, thus we do not provide additional details regarding their electronic spin states.

B. CALCULATION OF THE BINDING ENERGIES

In the following, we report the detailed calculation of the binding energies.

We are interested in the counterpoise-deformation-corrected interaction energy, where the basis set superposition error (BSSE) correction is included to make up for the error that arises when using a finite basis set of localized Gaussian functions to describe a chemical system:

$$\begin{aligned} \Delta E^{CP} &= \Delta E^* + \delta E_S + \delta E_\mu + \delta E_L - BSSE \\ &= \Delta E - BSSE \end{aligned} \quad (\text{B1})$$

From this equation it appears that the non-counterpoise-corrected interaction energy ΔE is given

by the sum of the deformation-free interaction energy (ΔE^*), the deformation energy of the slab (δE_S) and the molecule (δE_μ) and the lateral interaction (E_L) between adsorbate molecules in different replica of the cell. This quantity corresponds to the common definition of interaction energy, which is the difference between the energy of the complex and the energies of the isolated species and isolated ice model.

$$\begin{aligned} \Delta E &= \Delta E^* + \delta E_S + \delta E_\mu + \delta E_L \\ &= E_{\text{complex}} - E_{\text{ice}} - E_{\text{species}} \end{aligned} \quad (\text{B2})$$

The lateral interaction energy δE_L is due to the interactions experienced by each adsorbate with its images on the replicated unit cells. This term becomes particularly relevant for high adsorbate coverage, as the distances between adsorbate molecules in neighbour cells will become shorter with the increasing coverage. Here, we are interested in minimizing the δE_L term, to arrive to a ΔE representative of the sole interaction between the adsorbate and the ice surface. This requires the adoption of a large enough unit cell to minimize the δE_L term.

By convention, the binding energy is simply the opposite of ΔE^{CP} :

$$BE = -\Delta E^{CP} \quad (\text{B3})$$

Therefore, the $BE(0)$, that is the adsorption enthalpy at 0 K, can be obtained by simply subtracting the ZPE correction to the binding energy. In this work, we adopted $\Delta ZPE = ZPE_{\text{complex}} - ZPE_{\text{species}}$, where ZPE_{complex} was computed only for a fragment of the system constituted by the adsorbed species. In this way we are considering the same atoms in the two ZPE terms.

$$BE(0) = BE - \Delta ZPE \quad (\text{B4})$$

Species	Closed Shell Singlet	Open Shell Singlet	Triplet	Ring
S ₃	10	0	101	17
S ₄	43	0	21	60
S ₅	162	68	67	0

Table A2. Energy gaps (in kJ mol⁻¹) of sulphur allotropes computed in this work. The most stable structure is taken as the reference zero energy structure. The ring conformer possesses a closed shell singlet spin state. For S₅, the ring conformer consists in the envelope conformation.